

A Contour-Guided Deformable Image Registration Algorithm for Adaptive Radiotherapy

Xuejun Gu^{1,2}, Bin Dong^{1,3}, Jing Wang², John Yordy², Loren Mell¹, Xun Jia¹,
and Steve B. Jiang¹

5

¹Center for Advanced Radiotherapy Technologies and Department of Radiation
Medicine and Applied Sciences, University of California San Diego, La Jolla,
CA 92037-0843, USA

10

²Department of Radiation Oncology, The University of Texas Southwestern
Medical Center, Dallas TX, 75390 USA

³Department of Mathematics, The University of Arizona, Tucson, AZ, 85721-
0089, USA

15

E-mails: xuejun.gu@utsouthwestern.edu (Gu) and sbjiang@ucsd.edu (Jiang)

20

In adaptive radiotherapy, a deformable image registration is often conducted
between the planning CT and the treatment CT (or cone beam CT) to generate a
deformation vector field (DVF) for dose accumulation and contour propagation.
The auto-propagated contours on the treatment CT may contain relatively large
errors especially in low-contrast regions. Clinician's inspection and editing on
the propagated contours are always necessary. The edited contours are able to
meet the clinical requirement for adaptive therapy; however, the DVF is still
inaccurate and inconsistent with the edited contours. The purpose of this work is
to develop a contour-guided deformable image registration (CG-DIR) algorithm
to improve the accuracy and consistency of the DVF for adaptive radiotherapy.
The incorporation of the edited contours into the registration algorithm is
realized by regularizing the objective function of the original demons algorithm
with a term of intensity matching between the delineated structures set pairs.
The CG-DIR algorithm is implemented on computer graphics processing units
(GPUs) by following the original GPU-based demons algorithm computation
framework [Gu *et al*, Phys Med Biol. 55(1): 207-219, 2010]. The performance
of CG-DIR is evaluated on five clinical head-and-neck and one pelvic cancer
patient data. It is found that CG-DIR improves the accuracy and consistency of
the DVF when compared with the original demons, while keeps the high
computational efficiency of the original GPU-based demons.

35

1. Introduction

Deformable image registration (DIR) is a critical component in modern image-guided online and off-line adaptive radiation therapy (Yan, 2008). It is a process to precisely establish voxel-to-voxel correspondence of two images collected at different time or with different image modalities (Hill *et al.*, 2001; Crum *et al.*, 2004). The established correspondence, namely deformation vector field (DVF), has many applications in radiotherapy, such as facilitating auto-segmentation for anatomical changes (Brock *et al.*, 2005; Lu *et al.*, 2006; Rietzel and Chen, 2006; Chao *et al.*, 2008; Wang *et al.*, 2008; Xie *et al.*, 2008), estimating organ motion via 4D-CT images (Boldea *et al.*, 2008; Ehrhardt *et al.*, 2007; Yang *et al.*, 2008b; Zeng *et al.*, 2007), assisting the reconstruction of high-quality 4D-CT and CBCT images (Ren *et al.*, 2012; Wu *et al.*, 2011), calculating accumulated dose (Yan *et al.*, 1999; Rietzel *et al.*, 2005; Keall *et al.*, 2005), and *etc.* All applications rely on accurate DVFs generated by DIR algorithms.

During the past few decades, DIR has been studied in great detail and many algorithms have been proposed and developed (Holden, 2008; Kashani *et al.*, 2008; Crum *et al.*, 2004; Brock and Deformable Registration Accuracy Consortium, 2010). Among existing DIR algorithms, the image intensity based demons algorithm has been proven to be an efficient and robust algorithm (Pennec *et al.*, 1999; Wang *et al.*, 2005; Yang *et al.*, 2008a). Particularly, high computational efficiency is achieved by implementing demons algorithms on GPU (Gu *et al.*, 2010). In demons algorithm, the force to deform image is proportional to the gradients of moving and/or target image intensity. Therefore, the accuracy of estimating the images intensity gradient has great influence on the accuracy of image deformation and deforming those low-contrast and/or high-noise images with high accuracy is challenging by using demons algorithm (Nithianathan *et al.*, 2009; Yang *et al.*, 2008b; Zhong *et al.*, 2010).

In adaptive radiotherapy, DVFs generated in DIR algorithms are utilized mainly for dose accumulation and auto-contour propagation (Thor *et al.*, 2011). As uncertainties and errors exist in DVFs, the auto-propagated contours are apt to be distorted and hence required to be inspected and edited by physicians before their usage in treatment re-planning (Zhang *et al.*, 2007; Wang *et al.*, 2008; Reed *et al.*, 2009). Physicians' inputs correct the errors in contours generated by DVF, but not the errors in DVF itself. Then the dose accumulation is inaccurate due to the errors in DVF and also the DVF is inconsistent with the edited contours. In this paper, we propose to use edited contours to guide another run of DIR to reduce errors in DVF and increase consistency between DVF and final contours.

Studies of using contours to guide image registrations have been conducted for many years. For example, Shih *et al.* (Shih *et al.*, 1997) proposed an automated contour-model-guided DIR model to register a pair of MRI images. In the first step of their algorithm, authors established the geometric correspondence of contours in moving and reference MRI images. Then, based on the established correspondence, a non-linear transformation was determined using a weighted local coordinate system to deform the moving image. This algorithm is a pure geometrical-based image registration and the accuracy decreases

with the distance away from contour points. Later, Lie and Chuang (Lie and Chuang, 2003) designed a hybrid algorithm for thermographs deforming. They developed an algorithm combining the scheme of local contour matching and the method of global surface-spline fitting of control points. The registration accuracy achieved by their
 5 algorithm relies on the density of control points. Heavy computational burden arises when dense control points are used to ensure the registration accuracy.

In this paper, we propose a GPU-based contour-guided DIR (CG-DIR) algorithm, which honors global accuracy of registration and possess high computational efficiency as well. The CG-DIR model is a derivation of the demons algorithm, where the objective
 10 function of demon is revised, but the optimization scheme is unchanged. The objective function of the original demons has a term of summation of image intensity difference and a term of diffusion regularization of DVFs. In the proposed model, we add an additional regularization term using the regions of interest (ROIs) manifested by
 15 physicians' edited contours pairs. The optimization scheme is still the original demons iterative method, where a step of DVF updating and a step of DVF smoothing are performed at each iteration. With the preservation of the original GPU-based demons computational framework, GPU-based CG-DIR algorithm is able to achieve high
 20 computational efficiency. In this paper, we first detail the proposed CG-DIR model and its algorithm. Then, the performance of the new algorithm is quantitatively and qualitatively evaluated on five head-and-neck cancer patient data sets and one pelvic
 patient data set.

2. Methods and Materials

2.1 Contour-guided DIR model and algorithm

The goal of demons registration is to have the intensity matching between static and moving image through deforming moving image. The demon algorithm can be cast into a generalized optimization framework:

$$E(\mathbf{u}) = \frac{1}{2} \|I_0(\mathbf{x}) \circ \mathbf{u} - T_0(\mathbf{x})\|^2 + \frac{\alpha}{2} \|\nabla \mathbf{u}\|^2, \quad (1)$$

$$\mathbf{u} = \arg \min E(\mathbf{u})$$

30 Here, an optimal deformation vector field \mathbf{u} is estimated by minimizing an energy function between a moving image $I_0(\mathbf{x})$ and a target image $T_0(\mathbf{x})$. α is a regularization parameter for controlling the smoothness of \mathbf{u} over the image space.

In adaptive radiotherapy, $I_0(\mathbf{x})$ often represents a planning CT (pCT) image and $T_0(\mathbf{x})$ refers to a treatment CT (tCT) image. With physician delineated contours in pCT and edited contours in tCT, a constraint term defined by contours can be incorporated
 35 into equation (1) as:

$$E(\mathbf{u}) = \frac{1}{2} \|I_0(\mathbf{x}) \circ \mathbf{u} - T_0(\mathbf{x})\|^2 + \sum_{i=1}^k \frac{\lambda_i}{2} \|I_i(\mathbf{x}) \circ \mathbf{u} - T_i(\mathbf{x})\|^2 + \frac{\alpha}{2} \|\nabla \mathbf{u}\|^2, \quad (2)$$

$$\mathbf{u} = \arg \min E(\mathbf{u})$$

Here, $I_i(\mathbf{x})$ and $T_i(\mathbf{x})$ denote modified images constructed by incorporating i th contour pair set on pCT and tCT into original images $I_0(\mathbf{x})$ and $T_0(\mathbf{x})$, respectively; and k is the total number of modified contour pairs. The image modification is achieved with $I_i(\mathbf{x}) = \left(1 + \frac{M(\mathbf{x})}{2}\right)I_0(\mathbf{x})$ and $T_i(\mathbf{x}) = \left(1 + \frac{M(\mathbf{x})}{2}\right)T_0(\mathbf{x})$, where $M(\mathbf{x}) = \begin{cases} 1 & \mathbf{x} \in O_i \\ 0 & \text{else} \end{cases}$, and O_i represent a spatial domain that manifests a volume enclosed by i th contour pair on pCT and tCT. For simplification, we refer the volume enclosed by contours as an ROI and $I_i(\mathbf{x})$, $T_i(\mathbf{x})$ as modified images (MI). λ_i is a regularization parameter for each contour pair set, which controls the influence of ROI registration on the entire images registration.

Similar to the alternative optimization strategy proposed in Vercauteren *et al.* (Vercauteren *et al.*, 2009), an auxiliary variable \mathbf{c} is introduced to equation (2) to enable an relaxation minimization:

$$E(\mathbf{c}, \mathbf{u}) = \frac{1}{2} \|I_0(\mathbf{x}) \circ \mathbf{c} - T_0(\mathbf{x})\|^2 + \sum_{i=1}^k \frac{\lambda_i}{2} \|I_i(\mathbf{x}) \circ \mathbf{c} - T_i(\mathbf{x})\|^2 + \frac{\beta}{2} \|\mathbf{c} - \mathbf{u}\|^2 + \frac{\alpha}{2} \|\nabla \mathbf{u}\|^2, \quad (3)$$

$$(\mathbf{c}, \mathbf{u}) = \arg \min E(\mathbf{c}, \mathbf{u})$$

The algorithm is minimizing \mathbf{c} and \mathbf{u} in alternative steps. The first step takes optimization with a given \mathbf{u} : $\arg \min_{\mathbf{c}} E_1(\mathbf{c}) = \frac{1}{2} \|I_0(\mathbf{x}) \circ \mathbf{c} - T_0(\mathbf{x})\|^2 + \sum_{i=1}^k \frac{\lambda_i}{2} \|I_i(\mathbf{x}) \circ \mathbf{c} - T_i(\mathbf{x})\|^2 + \frac{\beta}{2} \|\mathbf{c} - \mathbf{u}\|^2$ and by making steps from $\mathbf{c} = \mathbf{u}$. The second step solves for the regularization by optimizing $\arg \min_{\mathbf{u}} E_2(\mathbf{u}) = \frac{\alpha}{2} \|\nabla \mathbf{u}\|^2 + \frac{\beta}{2} \|\mathbf{c} - \mathbf{u}\|^2$ with given \mathbf{c} . In the second step, an optimal regularization can be reached by the convolution of the deformation field \mathbf{u} with a Gaussian smoothing kernel $\mathbf{G}(\alpha)$ (Vercauteren *et al.*, 2009).

In the first step, given the current deformation \mathbf{u} , an updated (or displacement) deformation vector $d\mathbf{u}$ can be calculated by minimizing:

$$\arg \min_{d\mathbf{u}} E_1(d\mathbf{u}) = \frac{1}{2} \|I_0(\mathbf{x}) \circ (\mathbf{u} + d\mathbf{u}) - T_0(\mathbf{x})\|^2 + \sum_{i=1}^k \frac{\lambda_i}{2} \|I_i(\mathbf{x}) \circ (\mathbf{u} + d\mathbf{u}) - T_i(\mathbf{x})\|^2 + \frac{\beta}{2} \|d\mathbf{u}\|^2. \quad (4)$$

For a small displacement $d\mathbf{u}$, we can approximate the moving image term with a Taylor expansion: $I_0(\mathbf{x}) \circ (\mathbf{u} + d\mathbf{u}) \approx \tilde{I}_0(\mathbf{x}) + \nabla \tilde{I}_0(\mathbf{x}) \cdot d\mathbf{u}$ and $I_i(\mathbf{x}) \circ (\mathbf{u} + d\mathbf{u}) \approx \tilde{I}_i(\mathbf{x}) + \nabla \tilde{I}_i(\mathbf{x}) \cdot d\mathbf{u}$, where $\tilde{I}_0(\mathbf{x}) = I_0(\mathbf{x}) \circ \mathbf{u}$ and $\tilde{I}_i(\mathbf{x}) = I_i(\mathbf{x}) \circ \mathbf{u}$ are deformed moving images with given deformation \mathbf{u} . Then, equation (4) becomes:

$$\arg \min_{d\mathbf{u}} E_1(d\mathbf{u}) \approx \frac{1}{2} \|\tilde{I}_0(\mathbf{x}) + \nabla \tilde{I}_0(\mathbf{x}) \cdot d\mathbf{u} - T_0(\mathbf{x})\|^2 + \sum_{i=1}^k \frac{\lambda_i}{2} \|\tilde{I}_i(\mathbf{x}) + \nabla \tilde{I}_i(\mathbf{x}) \cdot d\mathbf{u} - T_i(\mathbf{x})\|^2 + \frac{\beta}{2} \|d\mathbf{u}\|^2 \quad (5)$$

In equation (5), we rewrite $\mathbf{du} = v\mathbf{n}$, where, v and \mathbf{n} are the amplitude and the moving direction of the displacement vector \mathbf{du} , respectively. Assuming that the displacement is determined on the projection \mathbf{du} onto $\mathbf{n} = \frac{\nabla \tilde{I}_0(\mathbf{x})}{|\nabla \tilde{I}_0(\mathbf{x})|}$ (Cachier *et al.*, 1999), the optimization problem defined in equation (5) can be simplified from $\mathbf{du} = \arg \min E(\mathbf{du})$ to $v = \arg \min E(v)$. Now the equation (5) becomes:

$$\arg \min_v E_1(v) \approx \frac{1}{2} \left\| (\nabla \tilde{I}_0(\mathbf{x}) \cdot \mathbf{n})v - (T_0(\mathbf{x}) - \tilde{I}_0(\mathbf{x})) \right\|^2 + \sum_{i=1}^k \frac{\lambda_i}{2} \left\| (\nabla \tilde{I}_i(\mathbf{x}) \cdot \mathbf{n})v - (T_i(\mathbf{x}) - \tilde{I}_i(\mathbf{x})) \right\|^2 + \frac{\beta v^2}{2} \quad (6)$$

Applying the first-order optimality condition $\frac{\partial E_1(v)}{\partial v} = 0$, we obtain a solution of equation (6):

$$v = \frac{(\nabla \tilde{I}_0(\mathbf{x}) \cdot \mathbf{n})(T_0(\mathbf{x}) - \tilde{I}_0(\mathbf{x})) + \sum_{i=1}^k \lambda_i (\nabla \tilde{I}_i(\mathbf{x}) \cdot \mathbf{n})(T_i(\mathbf{x}) - \tilde{I}_i(\mathbf{x}))}{(\nabla \tilde{I}_0(\mathbf{x}) \cdot \mathbf{n})^2 + \sum_{i=1}^k \lambda_i (\nabla \tilde{I}_i(\mathbf{x}) \cdot \mathbf{n})^2 + \beta}; \quad (7)$$

where β can be defined a spatial variable such as: $\beta = (T_0(\mathbf{x}) - \tilde{I}_0(\mathbf{x}))^2$ (Thirion, 1998).

10 2.2 Implementation of CG-DIR on GPU

As described in Section 2.1, CG-DIR is derived with a step of Taylor expansion and truncation, which implies that we can only allow a small and local displacement in registration. In order to reduce the magnitude of the displacement with respect to discretized image voxel size, a multi-scale strategy is adopted in CG-DIR algorithm. Registration iterations start with the lowest resolution, then the moving vectors obtained at a coarser level are up-sampled to serve as an initial solution at the next finer level. In this study, the entire registration is accomplished with two scales. The original images are only down-sampled once by a factor of 2 in each dimension. Further down-sampling was found neither to improve registration accuracy nor efficiency. In coarse resolution levels, demons registration is adopted to generate an approximate DVF. In the finest level, the moving vectors are updated by the proposed CG-DIR algorithm. One major reason of adopting demons in the coarse resolution level is to reduce computational burden. Also, the moving vectors obtained with demons in coarse resolution level are accurate enough to sever as an initial guess for the fine level CG-DIR registration.

Since the ROIs delineated by physicians are considered as the focus of our registration, the stopping criterion in CG-DIR is designed to emphasize on the registration accuracy of these ROIs. Each ROI is expanded with 1cm margin. The union of the expanded ROIs, referred to UROI in this paper, is the designed region to estimate the stopping metric. We defined a root mean square error of intensity difference (RMS-ID) at the k th iteration in UROI as: $\delta^k = \sqrt{1/N \sum (I^k(\mathbf{x}) - T(\mathbf{x}))^2}$, with $\mathbf{x} \in \text{UROI}$. Then, a stopping metric is chosen as the change of RMS-ID in successive iterations:

$l^{(k)} = \delta^k - \delta^{k-1}$, and use $l^{(k-10)} - l^{(k)} \leq \varepsilon$, where $\varepsilon = 1.0 \times 10^{-4}$, as our stopping criterion.

In the CG-DIR algorithm, there are three regularization parameters involved: α , β , and λ_i . These three regularization parameters have different functionality in the proposed CG-DIR algorithm. α , corresponding to the standard deviation of a Gaussian filter in our implementation, ensures a spatial smoothness of the deformation vector \mathbf{u} . In our study, we empirically choose a unit standard deviation for the Gaussian filter. β , related to image noise, is estimated locally as: $\beta = \left(T_0(\mathbf{x}) - \tilde{T}_0(\mathbf{x})\right)^2$ (Thirion, 1998; Vercauteren *et al.*, 2009). λ_i is a parameter designed to balance the registration efforts between the modified image pair and the original image pair. The value of λ_i depends on the intensity ratio between modified image ROIs and original image ROIs. In this work, the value of λ_i is found by a trail-and-error strategy and $\lambda_i \sim 1.0 \times 10^{-3}$ gives good deformation results for all cases studied.

The proposed CG-DIR algorithm was derived based on the original GPU-based demons algorithm (Gu *et al.*, 2010) and implemented on NVIDIA CUDA enabled GPU platform as well. We adopt the following data parallel GPU kernels including: kernel 1. **a low-pass filter kernel** to smooth images and deformation vectors; kernel 2. **a gradient kernel** to calculate the gradient of images; kernel 3. **a moving vector kernel** to calculate displacement vectors and update deformation vectors; kernel 4. **an interpolation kernel** to deform images with moving vectors and update moving vectors; kernel 5. **a comparison kernel** to calculate the stopping criteria to terminate iterations properly. Here, the low-pass filter kernel is accomplished by convolving the image with a three-dimensional Gaussian filter of a unit standard deviation. Taking advantage of the separability property of the Gaussian kernel, the convolution is implemented in x , y , and z directions sequentially.

Considering all components mentioned above, the CG-DIR algorithm is summarized as follows:

Algorithm A:

Initialization:

Set initial DVF $\mathbf{u}_0 := 0$;

Down-sample images $(I_0(\mathbf{x}), T_0(\mathbf{x}))$ to the coarsest resolution;

A. Coarse-level registration:

Perform demons registration between down-sampled $I_0(\mathbf{x})$ and $T_0(\mathbf{x})$ images;

Up-sample moving vector \mathbf{u} to a finer resolution level;

B. Finest-level registration:

Create modified images $I_i(\mathbf{x})$ and $T_i(\mathbf{x})$;

loop {over n until convergence}

1. Given the DVF at the n -th iteration \mathbf{u}^n , compute the displacement vector:

$$d\mathbf{u}^{n+1} = v^{n+1} \mathbf{n}^{n+1}, \text{ where } v^{n+1} \text{ is from eq. (7) and } \mathbf{n}^{n+1} = \frac{\nabla I_0^n(\mathbf{x})}{|\nabla I_0^n(\mathbf{x})|} \text{ (kernels 2 and 3);}$$

2. Smooth the displacement vector $d\mathbf{u}^{n+1} \leftarrow d\mathbf{u}^{n+1} \otimes \mathbf{G}$, here \mathbf{G} is a Gaussian

smoothing operator (kernel 1);

3. Update DVFs with a composite addition (Vercauteren *et al.*, 2009) $\mathbf{u}^{n+1} = \mathbf{u}^n \circ (\mathbf{I} + d\mathbf{u}^{n+1})$ (kernel 4), here \mathbf{I} is an identity matrix;
4. Smooth the updated DVF $\mathbf{u}^{n+1} = \mathbf{u}^{n+1} \otimes \mathbf{G}$ (kernel 1);
5. Warp images $I_0(\mathbf{x}) \circ \mathbf{u}^{n+1}$ and $I_i(\mathbf{x}) \circ \mathbf{u}^{n+1}$ (kernel 4);
6. Calculate $l^{(n)}$ to assess the stopping metric $l^{(n-10)} - l^{(n)} \leq \varepsilon$ (kernel 5).

end loop

2.3 Evaluation

The performance of CG-DIR is evaluated with clinical pCT and tCT image pairs for five head-and-neck cancer patients and one pelvis cancer patient. The tCT images were acquired 3-4 weeks after the first fraction of treatment due to the significant anatomy changes. In this study, both pCT and tCT images are segmented to exclude couch, masks, and other accessories. All DIR analysis is conducted on the segmented images. The original pCT and tCT images have dimensions around $\sim 512 \times 512 \times 150$. Due to the limitation of GPU memory, both tCT and pCT are down-sampled in axial planes and cropped in three dimensions. The images in this study have a resolution of $1.97 \times 1.97 \times 2.5$ mm³. Representative organs with low contrast image intensity to background such as GTV, parotids, rectum, and bladder were selected in this study for performing CG-DIR and for evaluating the results.

Direct evaluating DVF accuracy is difficult in clinical cases due to the lack of ground-truth DVFs. However, other information, such as image intensity, structure volume, and contours, is often available. Hence, indirect evaluation approaches through the usage of available ground-truth information is commonly adopted. More specifically, the calculated DVF is used to deform the image and ROI volumes, or to propagate the contours. Then, by assessing the difference between the deformed and the target image intensities, the overlapping rate of the deformed and the target ROI volumes, or the distance between the propagated contours and the target contours, the accuracy of DVF can be estimated.

In this study, the performance of the CG-DIR algorithm is first evaluated using image intensity difference. Two image intensity based assessment metrics are adopted: root mean square of intensity difference (RMS-ID) and correlation coefficient (CC) between the deformed pCT and the tCT. In this study, we calculate RMS-ID and CC over the entire image as well as the confined UROI.

The accuracy of the DVF resulted from the CG-DIR algorithm is further assessed using Dice Similarity Coefficient (DSC). DSC measuring volume overlapping, is a widely used similarity metric for evaluating deformable image registration results (Zhang *et al.*, 2007; Wang *et al.*, 2008; Xie *et al.*, 2008). DSC is defined as: $DSC = \frac{2(V_D \cap V_T)}{(V_D + V_T)}$, where V_D is the deformed volume of an ROI and V_T is the target volume of the same ROI. In this study V_T is the ROI volume enclosed by clinician manually edited contours. DCS

measures the volume overlap of V_D and V_T , zero indicating no overlapping and one indicating an exact volume match. In this work we apply this metric to solid organs like GTV and parotids.

5 The third type of comparison is contour matching, where the evaluated contours were propagated from pCT to tCT using the calculated DVF. Since DVFs generated by the CG-DIR algorithm only establish a 3D voxel-to-voxel correspondence map between pCT and tCT, when 2D axial-plane defined contour points on pCT are mapped onto rCT, points are easy to cross the plane. Such a point-to-point mapping will destroy points order in contour definition and generate non-smooth contours. Extra efforts are needed to
10 reorganize points and smooth contours. To avoid those extra tasks, we adopt a volume deformation strategy (Wang *et al.*, 2008): 1) deforming ROI volumes; 2) using morphological "opening" operation to remove small islands; 3) extracting boundary to obtain the propagated contours.

Quantitatively, the contours comparison is assessed with surface-to-surface distance (SSD), which is defined as the shortest Euclidean distance of the deformed points on contours to the target surface. In this study, the deformed contours of bladder and rectum are evaluated with this metric. The main reason is that the accurate deformation of organ walls rather than their fillers of these two organs are more critical in therapy treatment. In particular, we choose several basic statistical quantities of SSD to quantify the bladder and rectum deformation in a pelvic cancer case: 1) mean value of SSD (M-SSD) measuring how close the deformed surface to the target surface; 2) standard deviation of SSD values (SD-SSD) quantifying how deformed points scattered around M-SSD; and 3) 95 percentile SSD value gauging peak SSD values.

25 3. Experimental Results

The performance of CG-DIR algorithm is first assessed based on image intensity on five head-neck cancer patient cases and one pelvic cancer patient case. Figure 1 illustrates intensity difference images of an example case (Case HN 5). Before deformable image registration, a large discrepancy of image intensity is observed, as shown in Figure 1(a).
30 As the moving image is deformed by either demons algorithm or CG-DIR algorithm, the intensity inconsistency is greatly reduced, as shown in Figure 1(b) and (c). By comparing Figure 1(b) and (c), we can tell that these two difference images are very similar. We further illustrate intensity difference image between CG-DIR deformed image and demons deformed image in Figure 1(d). Quantitative evaluation of intensity difference of entire and regional registered image pairs is listed in Table 1. In this study, regional evaluation volume is chosen as UROI defined in Section 2.2.2. RMS-ID and CC values are very similar across these two algorithms, only slight improvement inside UROIs are observed by using CG-DIR algorithm in three out of 6 cases (HN 3, HN 4, and HN 5).
35 It is not surprise to see that intensity based metrics cannot differentiate these two algorithms. The CG-DIR algorithm focuses on improving DVFs accuracy regionally near delineated structure but does not disturb deformation of the entire image. Thus, close values of RMS-ID and CC of entire images between two algorithms are consistent with
40

the intention of algorithm design. Due to low contrast in UROIs, the accuracy improvement of DVFs will not have significant impact on image intensity maps, thus, intensity-based metrics, RMS-ID and CC, are not sensitive to improvement yield by CG-DIR algorithm.

5

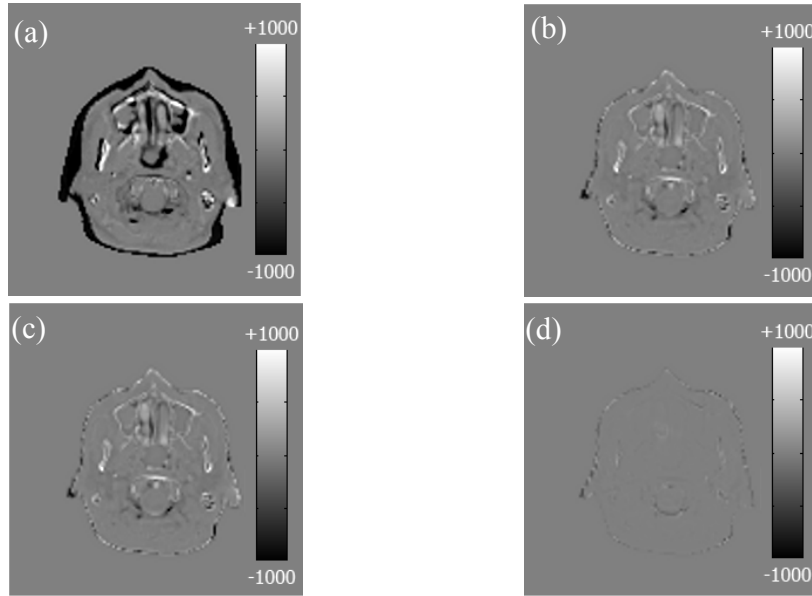


Figure 1. An example (Case HN 5) of difference image (scale in [-1000 1000] HU) at an axial cross section (a) between moving image and target image; (b) between demons deformed image and target image; (c) between CG-DIR deformed image and target image; and (d) between CG-DIR deformed image and demons deformed image.

Table 1. Root mean square of intensity difference and correlation coefficients of registered image pairs for six examined cases over entire image region (All) and in UROI.

| | | RMS-ID (HU) | | CC | |
|------|------|-------------|--------|--------|--------|
| | | Demons | CG-DIR | Demons | CG-DIR |
| HN 1 | All | 166.84 | 174.17 | 0.961 | 0.960 |
| | UROI | 2.58 | 2.82 | 0.927 | 0.923 |
| HN 2 | All | 68.00 | 68.36 | 0.994 | 0.990 |
| | UROI | 1.12 | 1.17 | 0.981 | 0.980 |
| HN 3 | All | 82.01 | 81.45 | 0.987 | 0.987 |
| | UROI | 0.73 | 0.70 | 0.978 | 0.979 |
| HN 4 | All | 74.87 | 72.97 | 0.980 | 0.983 |
| | UROI | 1.28 | 1.23 | 0.960 | 0.963 |
| HN 5 | All | 115.43 | 111.31 | 0.976 | 0.977 |
| | UROI | 0.31 | 0.30 | 0.947 | 0.951 |

| | | | | | |
|--------|------|-------|-------|-------|-------|
| Pelvic | All | 75.17 | 77.90 | 0.990 | 0.989 |
| | UROI | 0.23 | 0.23 | 0.923 | 0.923 |

Figure 2 shows an example result (Case HN 4), where manual drawn contours and auto-propagated contours are overlaid on tCT images. As we can see, big discrepancy exists between contours manually redrawn on tCT by physicians (blue lines) and those pCT contours mapped through rigid registration (red lines). This discrepancy is reduced when pCT contours is mapped through demons deformable registration (yellow lines). Further discrepancy reduction is achieved by mapping pCT contours through CG-DIR (green lines). This trend is quantitatively verified by examining the DSCs listed in Table 2. In our DSC evaluation, V_T is physicians delineated structure volumes on tCT and V_D is mapped (or deformed) structure volumes from pCT. As listed in Table 2, by applying rigid registration to map contours, the mean DSC value for evaluated structures varies from 0.02 ~ 0.40 (average, 0.25). The values of DSC increase to 0.7~0.9 when V_D is demons deformed ROI volume. Further increasing of DSC to ~0.98 was observed when deforming ROI volume with CG-DIR algorithm.

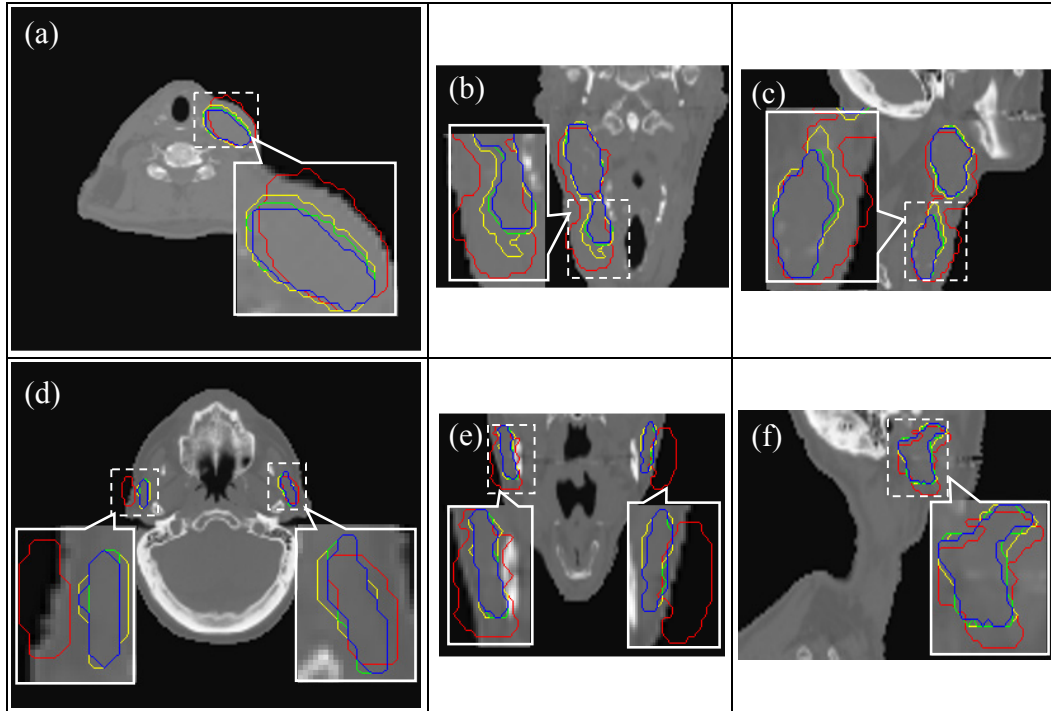


Figure 2. GTV and parotid contours overlaid on tCT (a), (d) axial, (b), (e) coronal, and (c), (f) sagittal images for case HN4. Here, (a), (b) and (c) show GTV contours and (d), (e), (f) show parotid contours. Red lines: manual contours on pCT and mapped on tCT through rigid registration. Blue lines: manually edited contours on tCT. Yellow line: deformed pCT contours through demons registration. Green line: deformed pCT contours through CG-DIR registration.

Table 2. Dice similarity coefficients between physicians' manually delineated parotids and GTV

volumes and mapped volumes using different registration algorithms.

| | | Rigid Registration | Demons | CG-DIR |
|------|---------------|--------------------|--------|--------|
| HN 1 | Left Parotid | 0.03 | 0.70 | 0.94 |
| | Right Parotid | 0.02 | 0.92 | 0.97 |
| HN 2 | Left Parotid | 0.39 | 0.94 | 0.98 |
| | Right Parotid | 0.42 | 0.90 | 0.97 |
| HN 3 | Left Parotid | 0.33 | 0.94 | 0.99 |
| | Right Parotid | 0.30 | 0.95 | 0.99 |
| HN 4 | Left Parotid | 0.27 | 0.90 | 0.96 |
| | Right Parotid | 0.07 | 0.94 | 0.98 |
| | GTV | 0.32 | 0.89 | 0.97 |
| HN 5 | Left Parotid | 0.29 | 0.89 | 0.95 |
| | Right Parotid | 0.24 | 0.94 | 0.98 |
| | GTV | 0.40 | 0.95 | 0.99 |

Further evaluation of the CG-DIR algorithm is conducted on a pelvic cancer patient case using SSD. Figure 3 illustrates mapped and manually drawn contours overlaid on tCT images. From visual inspection, the CG-DIR mapped contours have the best agreement with manual tCT contours, and the rigid mapping has the worst one. Quantitative measurement of contours agreement is given by calculating SSD. Table 3 lists some basic statistical values of SSD, including mean, standard deviation, 95 percentile. As shown in Table 3, 95 percentile errors of wrapped bladder and rectum surface points have errors around 2~3mm, which indicates that only 5% points on wrapped surfaces have errors larger than a voxel size. In contrast, demons wrapped surfaces have errors larger than a voxel size. In contrast, demons wrapped surfaces have a relative large error, where 95% percentile errors are 3~4 voxel size.

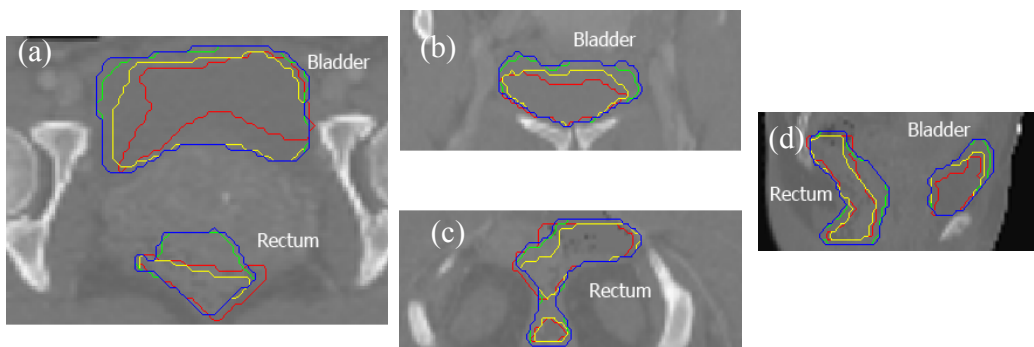


Figure 3. The bladder and rectum contours overlaid on tCT (a) axial, (b), (c) coronal, and (d) sagittal images for the pelvic case. (b) and (c) show coronal cross-section for bladder and rectum contours respectively. Red lines: manual contours on pCT and mapped on tCT through rigid

registration. Blue lines: manual contours on tCT. Yellow line: deformed contours through demons registration. Green line: deformed contours through CG-DIR registration.

Table 3. Statistical function of SSD between clinician manually delineated rectum and bladder contours and mapped contours using different registration algorithms

| SSD (mm) | Demons | | | CG-DIR | | |
|----------------|--------|-----------------------|------------------|--------|-----------------------|------------------|
| | Mean | Standard Deviation | 95 percentile | Mean | Standard Deviation | 95 percentile |
| Bladder | 2.75 | 5.80 | 7.81 | 0.74 | 1.09 | 3.09 |
| Rectum | 2.44 | 2.66 | 8.29 | 0.48 | 0.74 | 1.95 |

5

As mentioned above, our CG-DIR algorithm is derived from the demons algorithm and its implementation follows the original demons computational framework. (Gu *et al.*, 2010). Compared to the original demons algorithm, our CG-DIR algorithm has three extra computational components at each iteration for vector field updating: 1) enhanced image gradient calculation; 2) enhanced image deformation; 3) composite moving vector calculation using equation (7). Along with these extra computational components, our CG-DIR algorithm has a high requirement of graphic memory, due to additional variables needed to store enhanced image, their gradient fields, as well as a binary UROI map used in calculating stopping criteria. The performance of the developed CG-DIR algorithm was conducted on an NVIDIA Tesla C1060 card. This card is equipped with 240 1.3GHz stream processors and 4 GB graphic memory. Due to additional computational steps, the computational time is expected to be longer than the GPU-based original demons. In the tested 6 cases, the computational time for each CG-DIR iteration is about 1.3~1.6 times more than that of the original demons. For example, case HN 4 has an image size of 240×160×70, and it takes around 55 msec for each CG-DIR iteration compared to 42 msec for each demons iteration.

10

15

20

4. Discussion

25

30

In image-guided adaptive radiotherapy, DIR is an essential tool for automated organ delineation, dose accumulation, and 4D treatment planning. Although this imaging tool works well with certain cases such as high-contrast thoracic 4D-CT images, it may generate DVFs with large uncertainties and errors in low-contrast regions leading to distortion in auto-propagated contour. Thus, manual contour inspection and editing is always necessary. The proposed CG-DIR algorithm incorporates the physician-edited contours into an additional deformable registration to reduce the errors in DVF and to improve the consistency between the DVF and the edited contours. This DVF correction is crucial for later dose accumulation in adaptive therapy or accurate 4D treatment planning.

The contour-guided deformable image registration algorithm developed in this paper has an underlying assumption that contours edited by physicians are accurate. Intra-observer contouring variations exist in real clinical situations, which could lead to uncertainties in contours correction and subsequently DVF correction. However, the application of CG-DIR algorithm in adaptive radiotherapy is under the scenario that physicians edit auto-propagated contours. Edited contours have much less variation than those independently drawn contours from scratch (Wang *et al.*, 2008). Hence, intra-observer variation will unlikely be a big issue for the CG-DIR application.

The computational efficiency of CG-DIR has room to be further improved. Under the scenario that physicians editing contours based on auto-propagated contours, the registration in coarse-level with demons can be eliminated. The DVF generated during the auto-contouring can be used as an initial DVF value for CG-DIR and thus practically there is no need for coarse level registration. Regarding the memory usage of CG-DIR, in this study, each delineated structure has its own modified image, which is a memory-consuming strategy. The usage of GPU-based CG-DIR algorithm is limited by available memory space on a graphic card. As mentioned above, compared to demons algorithm, CG-DIR algorithm requires extra memory to store auxiliary variables. On a Telsa C1060 card, 4GB graphic memory allows us to handle images with a size $\sim 256 \times 256 \times 70$ and two delineated organs. Further investigation of optimizing memory usage is needed for applying this algorithm to CT data sets of larger size.

Another issue in the CG-DIR algorithm is the selection of a proper regularization parameter λ . In this study, we use a trial-and-error method to find a good λ value for each study case. According to our observation, λ values are relatively consistent for all studied cases. Additional comprehensive image datasets for other anatomical regions are needed for further investigations to confirm the findings presented here.

5. Conclusions

A contour-guided deformable image registration algorithm has been developed and validated for adaptive radiotherapy. Physician edited contours in conjugated with images intensity are employed to deform image more accurately and results in DVFs more consistent with physicians edited contours. The developed CG-DIR algorithm has been applied to patient studies resulting in an improvement of the DVF accuracy at a high computational efficiency.

Acknowledgements

This work is supported in part by the University of California Lab Fees Research Program and by an NIH/NCI grant 2F32 CA154045-01.

References

- Boldea V, Sharp G C, Jiang S B and Sarrut D 2008 4D-CT lung motion estimation with deformable registration: Quantification of motion nonlinearity and hysteresis *Medical Physics* **35** 1008-18
- 5 Brock K K and Deformable Registration Accuracy Consortium 2010 Results of a multi-institution deformable registration accuracy study (MIDRAS) *International Journal of Radiation Oncology Biology Physics* **76** 583-96
- Brock K K, Sharpe M B, Dawson L A, Kim S M and Jaffray D A 2005 Accuracy of finite element model-based multi-organ deformable image registration
- 10 *Medical Physics* **32** 1647-59
- Cachier P, Pennec X and Ayache N 1999 Fast non-rigid matching by gradient descent: study and improvement of the 'Demons' algorithm *Technical Report INRIA RR-3706*
- Chao M, Xie Y Q and Xing L 2008 Auto-propagation of contours for adaptive prostate radiation therapy *Phys. Med. Biol.* **53** 4533-42
- 15 Crum W R, Hartkens T and Hill D L G 2004 Non-rigid image registration: theory and practice *British Journal of Radiology* **77** S140-S53
- Ehrhardt J, Werner R, Saering D, Frenzel T, Lu W, Low D and Handels H 2007 An optical flow based method for improved reconstruction of 4D CT data sets acquired during free breathing *Medical Physics* **34** 711-21
- 20 Gu X J, Pan H, Liang Y, Castillo R, Yang D S, Choi D J, Castillo E, Majumdar A, Guerrero T and Jiang S B 2010 Implementation and evaluation of various demons deformable image registration algorithms on a GPU *Phys. Med. Biol.* **55** 207-19
- 25 Hill D L G, Batchelor P G, Holden M and Hawkes D J 2001 Medical image registration *Phys. Med. Biol.* **46** R1-R45
- Holden M 2008 A review of geometric transformations for nonrigid body registration *Ieee Transactions on Medical Imaging* **27** 111-28
- Kashani R, Hub M, Balter J M, Kessler M L, Dong L, Zhang L, Xing L, Xie Y,
- 30 Hawkes D, Schnabel J A, McClelland J, Joshi S, Chen Q and Lu W 2008 Objective assessment of deformable image registration in radiotherapy: A multi-institution study *Medical Physics* **35** 5944-53
- Keall P J, Joshi S, Vedam S S, Siebers J V, Kini V R and Mohan R 2005 Four-dimensional radiotherapy planning for DMLC-based respiratory motion tracking *Medical Physics* **32** 942-51
- 35 Lie W N and Chuang C H 2003 Contour-based image registration with local deformations *Optical Engineering* **42** 1405-16
- Lu W G, Olivera G H, Chen Q, Chen M L and Ruchala K J 2006 Automatic re-contouring in 4D radiotherapy *Phys. Med. Biol.* **51** 1077-99
- 40 Nithianathan S, Brock K K, Daly M J, Chan H, Irish J C and Siewerdsen J H 2009 Demons deformable registration for CBCT-guided procedures in the head and neck: Convergence and accuracy *Medical Physics* **36** 4755-64
- Pennec X, Cachier P and Ayache N 1999 Understanding the "Demon's Algorithm": 3D Non-Rigid registration by Gradient Descent. In: *2nd int. conf. on medical image computing and computer-assisted intervention (MICCAI'99) LNCS*, pp 597-605
- 45

- Reed V K, Woodward W A, Zhang L, Strom E A, Perkins G H, Tereffe W, Oh J L, Yu T K, Bedrosian I, Whitman G J, Buchholz T A and Dong L 2009 Automatic Segmentation of whole breast using atlas approach and deformable image registration *International Journal of Radiation Oncology Biology Physics* **73** 1493-500
- 5 Ren L, Chetty I J, Zhang J N, Jin J Y, Wu Q J, Yan H, Brizel D M, Lee W R, Movsas B and Yin F F 2012 Development and clinical evaluation of a three-dimensional cone-beam computed tomography estimation method using a deformation field map *International Journal of Radiation Oncology Biology Physics* **82** 1584-93
- 10 Rietzel E and Chen G T Y 2006 Deformable registration of 4D computed tomography data *Medical Physics* **33** 4423-30
- Rietzel E, Chen G T Y, Choi N C and Willet C G 2005 Four-dimensional image-based treatment planning: Target volume segmentation and dose
- 15 calculation in the presence of respiratory motion *International Journal of Radiation Oncology Biology Physics* **61** 1535-50
- Shih W-S V, Lin W-C and Chen C-T 1997 Contour-model-guided nonlinear deformation model for inter-subject image registration *Proceedings of the SPIE - The International Society for Optical Engineering* **3034**
- 20 Thirion J P 1998 Image matching as a diffusion process: an analogy with Maxwell's demons *Med Image Anal* **2** 243-60
- Thor M, Petersen J B B, Bentzen L, Hoyer M and Muren L P 2011 Deformable image registration for contour propagation from CT to cone-beam CT scans in radiotherapy of prostate cancer *Acta Oncologica* **50** 918-25
- 25 Vercauteren T, Pennec X, Perchant A and Ayache N 2009 Diffeomorphic demons: Efficient non-parametric image registration *Neuroimage* **45** S61-S72
- Wang H, Adam S G, Zhang L F, Wei X, Ahamad A, Kuban D A, Komaki R, O'Daniel J, Zhang Y B, Mohan R and Dong L 2008 Performance
- 30 evaluation of automatic anatomy segmentation algorithm on repeat or four-dimensional computed tomography images using deformable image registration method *International Journal of Radiation Oncology Biology Physics* **72** 210-9
- Wang H, Dong L, O'Daniel J, Mohan R, Garden A S, Ang K K, Kuban D A, Bonnen M, Chang J Y and Cheung R 2005 Validation of an accelerated 'demons' algorithm for deformable image registration in radiation therapy
- 35 *Physics in Medicine and Biology* **50** 2887-905
- Wu G, Wang Q, Lian J and Shen D 2011 Reconstruction of 4D-CT from a single free-breathing 3D-CT by spatial-temporal image registration *Information processing in medical imaging : proceedings of the ... conference* **22** 686-98
- 40 Xie Y, Chao M, Lee P and Xing L 2008 Feature-based rectal contour propagation from planning CT to cone beam CT *Medical Physics* **35** 4450-9
- 45 Yan D 2008 Developing quality assurance processes for image-guided adaptive radiation therapy *Int J Radiat Oncol Biol Phys* **71** S28-32

- Yan D, Jaffray D A and Wong J W 1999 A model to accumulate fractionated dose in a deforming organ *International Journal of Radiation Oncology Biology Physics* **44** 665-75
- 5 Yang D, Li H, Low D A, Deasy J O and Naqa I E 2008a A fast inverse consistent deformable image registration method based on symmetric optical flow computation *Physics in Medicine and Biology* **53** 6143-65
- Yang D S, Lu W, Low D A, Deasy J O, Hope A J and El Naqa I 2008b 4D-CT motion estimation using deformable image registration and 5D respiratory motion modeling *Medical Physics* **35** 4577-90
- 10 Zeng R P, Fessler J A and Balter J M 2007 Estimating 3-D respiratory motion from orbiting views by tomographic image registration *Ieee Transactions on Medical Imaging* **26** 153-63
- Zhang T, Chi Y, Meldolesi E and Yan D 2007 Automatic delineation of on-line head-and-neck computed tomography images: Toward on-line adaptive radiotherapy *International Journal of Radiation Oncology Biology Physics* **68** 522-30
- 15 Zhong H L, Kim J and Chetty I J 2010 Analysis of deformable image registration accuracy using computational modeling *Medical Physics* **37** 970-9

20